Pramana – J. Phys. (2018) 91:59
https://doi.org/10.1007/s12043-018-1631-0

Numerical solutions of the Gardner equation by extended form of the cubic B-splines

OZLEM ERSOY HEPSON[1,*], ALPER KORKMAZ[2] and IDRIS DAG[3]

[1]Mathematics and Computer Department, Eskişehir Osmangazi University, Eskişehir, Turkey
[2]Department of Mathematics, Çankırı Karatekin University, Çankırı, Turkey
[3]Computer Engineering Department, Eskişehir Osmangazi University, Eskişehir, Turkey
[*]Corresponding author. E-mail: ozersoy@ogu.edu.tr

MS received 20 October 2017; revised 2 March 2018; accepted 23 March 2018; published online 25 August 2018

Abstract. The extended definition of the polynomial B-splines may give a chance to improve the results obtained by the classical cubic polynomial B-splines. The optimum value of the extension parameter can be determined by scanning some intervals containing zero. This study aims to solve some initial boundary value problems constructed for the Gardner equation by the extended cubic B-spline collocation method. The test problems are derived from some analytical studies to validate the efficiency and accuracy of the suggested method. The conservation laws are also determined to observe whether the test problems remain constant as expected from the theoretical aspect. The stability of the proposed method is investigated by the von Neumann analysis.

Keywords. Gardner equation; soliton; perturbation; wave generation; extended B-spline.

PACS Nos 04.30.Db; 05.45.Yv; 02.60.Cb; 02.70.Jn

1. Introduction

Consider the Gardner equation (or the combined Korteweg–de Vries (KdV)-modified Korteweg–de Vries (mKdV)) of the following form:

$$u_t + \mu_1 u u_x + \mu_2 u^2 u_x + \mu_3 u_{xxx} = 0, \tag{1}$$

where $u = u(x,t)$ and μ_1, μ_2 and μ_3 are constants. The Gardner equation has two nonlinear terms in the quadratic and cubic forms and the dissipative term is of third order. The Gardner equation is an integrable system and the Miura transformation connects it to the KdV equation [1].

The Gardner equation is a useful model to understand the propagation of negative ion-acoustic plasma waves [2]. The equation can be derived from the system of plasma motion equations in one dimension with arbitrarily charged cold ions and inertia-neglected isothermal electrons.

The Gardner equation can also be a good description of the internal waves with large amplitudes [3]. The modulation system in the Riemann invariant form and classified solutions for large t values subject to some particular initial conditions are studied thoroughly to explain the undular bore formation. The structure of the nonlinear terms are significant for the solution classification. The sign of μ_2 also has a critical role for the structures of the solutions. The patterns of the solutions can be either bright or dark cnoidal or trigonometric bores, kinks, rarefaction waves or their combinations.

Some particular forms of the internal ocean rogue waves in the coasts occur in the Gardner equation when μ_2 and μ_3 have the same sign which enables modulational instability [4]. The Gardner equation can also be a useful model to study stratified fluid transcritical flow passing a topographic obstacle when a forcing term is added to the equation [5].

An interacting two-soliton-type solution is derived by Darboux transformations in Slyunyaev and Pelinovskii's study [6]. The consistent tanh method is also capable of generating interacting solutions to the Gardner equation [7]. Some interactions of two-wave solutions such as a soliton–cnoidal wave or a soliton–periodic wave are presented in this study. The consistent Riccati expansion is another method that is capable of obtaining soliton–cnoidal wave interaction-type solutions [8].

In the adiabatic parameter case, the dynamics of the solitons of the perturbed Gardner equation was

studied in detail by Biswas and Zerrad [9]. The motion integrals are also determined for the perturbed form of the equation. The effects of perturbation on a single-soliton-type solution are discussed by considering the tanh-type initial data [10]. A travelling solitary wave solution of the type of the singularly perturbed Gardner equation was derived in [11] and the solutions were verified numerically.

Exact solutions to the Gardner equation are set up by using various methods. Some solutions containing tanh and coth functions are proposed by the extended form of the tanh method [12]. The solitary wave and periodic solutions are constructed by using projective Riccati equations [13]. These solutions have various terms including trigonometric or hyperbolic functions in rational forms. G'/G is another expansion method to determine exact solutions to the Gardner equation. Some solitary, periodic, exponential, rational and complex-type travelling wave solutions are obtained by this method [14]. Some other exact solutions in terms of trigonometric functions [15–17], hyperbolic functions [15,16,18] and kink solutions [19] are determined by using different expansion or ansatz methods.

Numerical solutions to the Gardner and Gardner-like equations are also considered in various studies. The conservative finite-difference scheme is developed to determine the propagation of one-soliton and collusion of two-soliton solutions numerically [20]. A restrictive Taylor's technique has also been implemented to simulate the propagation of some solutions numerically [21]. A recent study also has dealt with the Gardner equation by solving it numerically using the finite-element method based on polynomial quintic B-splines [22]. Various bright methods have been implemented to Gardner-like equations to solve different initial boundary value problems [23,24].

In the present study, we develop an extended cubic B-spline collocation method to the solutions of the Gardner equation. Since the cubic B-splines are twice continuously differentiable, the order of the Gardner equation is reduced by defining the splitting $v = u_x$ so that the obtained coupled system of order two can be solved by using extended cubic B-spline collocation method.

$$u_t+(\mu_1 u+\mu_2 u^2)u_x+\mu_3, \quad v_{xx}=0, \quad v-u_x=0. \tag{2}$$

In order to complete the mathematical notation of the initial boundary value problems, we use the initial data

$$u(x,0)=f(x), \quad v(x,0)=f_x(x) \tag{3}$$

and the homogeneous Neumann conditions

$$\begin{aligned} &u_x(a,t)=0, \quad u_x(b,t)=0,\\ &u_{xx}(a,t)=0, \quad u_{xx}(b,t)=0,\\ &v_x(a,t)=0, \quad v_x(b,t)=0,\\ &v_{xx}(a,t)=0, \quad v_{xx}(b,t)=0 \end{aligned} \tag{4}$$

at both ends of the problem interval $[a,b]$.

2. Numerical approximate

Consider the equal grid distribution

$$\pi : a=x_0<x_1<\cdots<x_N=b$$

of the finite interval $[a,b]$, where $h=(b-a)/N$ is the equal mesh size. An extended B-spline function is defined as

$$E_j(x)=\frac{1}{24h^4}\begin{cases} 4h(1-\lambda)(x-x_{j-2})^3+3\lambda(x-x_{j-2})^4, & [x_{j-2},x_{j-1}],\\ (4-\lambda)h^4+12h^3(x-x_{j-1})+6h^2(2+\lambda)(x-x_{j-1})^2 & \\ -12h(x-x_{j-1})^3-3\lambda(x-x_{j-1})^4, & [x_{j-1},x_i],\\ (4-\lambda)h^4-12h^3(x-x_{j+1})+6h^2(2+\lambda)(x-x_{j+1})^2 & \\ +12h(x-x_{j+1})^3-3\lambda(x-x_{j+1})^4, & [x_i,x_{j+1}],\\ 4h(\lambda-1)(x-x_{j+2})^3+3\lambda(x-x_{j+2})^4, & [x_{j+1},x_{j+2}],\\ 0 & \text{otherwise.}\end{cases} \tag{5}$$

with the extension parameter λ. In fact, the classical cubic polynomial B-splines are the particular form of the extended cubic B-splines when $\lambda=0$. The set of extended B-spline functions $\{E_{-1}(x),E_0(x),\ldots,E_{N+1}(x)\}$ constitutes a basis function set for the functions defined in this interval. The approximate solutions $U(x,t)$ and $V(x,t)$ to $u(x,t)$ and $v(x,t)$, respectively, can be written in terms of the extended B-splines as

$$U(x,t)=\sum_{j=-1}^{N+1}\delta_j E_j(x), \quad V(x,t)=\sum_{j=-1}^{N+1}\phi_j E_j(x), \tag{6}$$

where δ_j and ϕ_j are time-dependent parameters. These parameters are determined after the implementation of the collocation method. The nodal derivative values of both U and V can be summarised in terms of the extended B-splines as

$$
\begin{aligned}
U_j &= U(x_j,t) = \frac{4-\lambda}{24}\delta_{j-1} + \frac{8+\lambda}{12}\delta_j + \frac{4-\lambda}{24}\delta_{j+1},\\
V_j &= V(x_j,t) = \frac{4-\lambda}{24}\phi_{j-1} + \frac{8+\lambda}{12}\phi_j + \frac{4-\lambda}{24}\phi_{j+1},\\
U'_j &= U'(x_j,t) = \frac{-1}{2h}(\delta_{j-1} - \delta_{j+1}),\\
V'_j &= V'(x_j,t) = \frac{-1}{2h}(\phi_{j-1} - \phi_{j+1}),\\
U''_j &= U''(x_j,t) = \frac{2+\lambda}{2h^2}(\delta_{j-1} - 2\delta_j + \delta_{j+1}),\\
V''_j &= V''(x_j,t) = \frac{2+\lambda}{2h^2}(\phi_{j-1} - 2\phi_j + \phi_{j+1}). \qquad (7)
\end{aligned}
$$

The time integration of the space-splitted system (2) is performed by the Crank–Nicolson method as

$$
\begin{aligned}
&\frac{U^{n+1}-U^n}{\Delta t} + \mu_1\frac{(UU_x)^{n+1}+(UU_x)^n}{2}\\
&\quad + \mu_2\frac{(U^2U_x)^{n+1}+(U^2U_x)^n}{2} + \mu_3\frac{V_{xx}^{n+1}+V_{xx}^n}{2} = 0,\\
&\frac{V^{n+1}+V^n}{2} - \frac{U_x^{n+1}+U_x^n}{2} = 0, \qquad (8)
\end{aligned}
$$

where the superscript n represents the solution at the nth time level with equal time step size Δt satisfying $t^{n+1} = t^n + \Delta t$.

The nonlinear terms $(UU_x)^{n+1}$ and $(U^2U_x)^{n+1}$ in eq. (8) are converted to linear forms by using

$$
(UU_x)^{n+1} = U^{n+1}U_x^n + U^nU_x^{n+1} - U^nU_x^n
$$

and

$$
\begin{aligned}
(U^2U_x)^{n+1} &= 2U^{n+1}U^nU_x^n + (U^n)^2U_x^{n+1}\\
&\quad - 2(U^n)^2U_x^n
\end{aligned}
$$

defined in [25]. The resultant linear system is discretised in space by using the extended cubic collocation method as

$$
\begin{aligned}
&\left[\left(\frac{2}{\Delta t}+\mu_1L+2\mu_2KL\right)\alpha_1+(\mu_1+\mu_2K)\,K\beta_1\right]\delta_{j-1}^{n+1}\\
&\quad+[\mu_3\gamma_1]\phi_{j-1}^{n+1}+\left[\left(\frac{2}{\Delta t}+\mu_1L+2\mu_2KL\right)\alpha_2\right]\delta_j^{n+1}\\
&\quad+[\mu_3\gamma_2]\phi_j^{n+1}+\left[\left(\frac{2}{\Delta t}+\mu_1L+2\mu_2KL\right)\alpha_1\right.\\
&\quad\left.-(\mu_1+\mu_2K)\,K\beta_1\right]\delta_{j+1}^{n+1}+[\mu_3\gamma_1]\phi_{j+1}^{n+1}\\
&=\left[\left(\frac{2}{\Delta t}+\mu_2KL\right)\alpha_1\right]\delta_{j-1}^n-\mu_3\gamma_1\phi_{j-1}^n\\
&\quad+\left[\left(\frac{2}{\Delta t}+\mu_2KL\right)\alpha_2\right]\delta_j^n-\mu_3\gamma_2\phi_j^n\\
&\quad+\left[\left(\frac{2}{\Delta t}+\mu_2KL\right)\alpha_1\right]\delta_{j+1}^n-\mu_3\gamma_1\phi_{j+1}^n-\beta_1\delta_{j-1}^{n+1}\\
&\quad+\alpha_1\phi_{j-1}^{n+1}+\alpha_2\phi_j^{n+1}+\beta_1\delta_{j+1}^{n+1}+\alpha_1\phi_{j+1}^{n+1},\\
&=\beta_1\delta_{j-1}^n-\alpha_1\phi_{j-1}^n-\alpha_2\phi_j^n-\beta_1\delta_{j+1}^n-\alpha_1\phi_{j+1}^n,\\
&\quad m=0,\ldots,N,\quad n=0,1,\ldots, \qquad (9)
\end{aligned}
$$

where

$$
\begin{aligned}
K &= \alpha_1\delta_{j-1}^n+\alpha_2\delta_j^n+\alpha_1\delta_{j+1}^n,\\
L &= \alpha_1\phi_{j-1}^n+\alpha_2\phi_j^n+\alpha_1\phi_{j+1}^n,\\
\alpha_1 &= \frac{4-\lambda}{24},\quad \alpha_2 = \frac{8+\lambda}{12},\\
\beta_1 &= -\frac{1}{2h},\quad \gamma_1 = \frac{2+\lambda}{2h^2},\quad \gamma_2 = -\frac{4+2\lambda}{2h^2}.
\end{aligned}
$$

This system can be written in the matrix notation as

$$
\mathbf{A}\mathbf{x}^{n+1} = \mathbf{B}\mathbf{x}^n, \qquad (10)
$$

where

$$
\mathbf{A} = \begin{bmatrix}
\nu_1 & \nu_2 & \nu_3 & \nu_4 & \nu_5 & \nu_2 & & & & \\
-\beta_1 & \alpha_1 & 0 & \alpha_2 & \beta_1 & \alpha_1 & & & & \\
 & & \nu_1 & \nu_2 & \nu_3 & \nu_4 & \nu_5 & \nu_2 & & \\
 & & -\beta_1 & \alpha_1 & 0 & \alpha_2 & \beta_1 & \alpha_1 & & \\
 & & & \ddots & \ddots & \ddots & \ddots & \ddots & \ddots & \\
 & & & & \nu_1 & \nu_2 & \nu_3 & \nu_4 & \nu_5 & \nu_2 \\
 & & & & -\beta_1 & \alpha_1 & 0 & \alpha_2 & \beta_1 & \alpha_1
\end{bmatrix},
$$

$$
\mathbf{B} = \begin{bmatrix}
\nu_6 & -\nu_2 & \nu_7 & -\nu_4 & \nu_6 & -\nu_2 & & & & \\
\beta_1 & -\alpha_1 & 0 & -\alpha_2 & -\beta_1 & -\alpha_1 & & & & \\
 & & \nu_6 & -\nu_2 & \nu_7 & -\nu_4 & \nu_6 & -\nu_2 & & \\
 & & \beta_1 & -\alpha_1 & 0 & -\alpha_2 & -\beta_1 & -\alpha_1 & & \\
 & & & \ddots & \ddots & \ddots & \ddots & \ddots & \ddots & \\
 & & & & \nu_6 & -\nu_2 & \nu_7 & -\nu_4 & \nu_6 & -\nu_2 \\
 & & & & \beta_1 & -\alpha_1 & 0 & -\alpha_2 & -\beta_1 & -\alpha_1
\end{bmatrix}
$$

and

$$\nu_1 = \left(\frac{2}{\Delta t} + \mu_1 L + 2\mu_2 KL\right)\alpha_1 + (\mu_1 K + \mu_2 K^2)\beta_1,$$
$$\nu_2 = \mu_3 \gamma_1,$$
$$\nu_3 = \left(\frac{2}{\Delta t} + \mu_1 L + 2\mu_2 KL\right)\alpha_2,$$
$$\nu_4 = \mu_3 \gamma_2,$$
$$\nu_5 = \left(\frac{2}{\Delta t} + \mu_1 L + 2\mu_2 KL\right)\alpha_1 - (\mu_1 K + \mu_2 K^2)\beta_1,$$
$$\nu_6 = \left(\frac{2}{\Delta t} + \mu_2 KL\right)\alpha_1,$$
$$\nu_7 = \left(\frac{2}{\Delta t} + \mu_2 KL\right)\alpha_2.$$

System (10) consists of $2N + 2$ linear equations and $2N + 6$ unknowns

$$\mathbf{x}^{n+1} = (\delta_{-1}^{n+1}, \phi_{-1}^{n+1}, \delta_0^{n+1}, \phi_0^{n+1}, \ldots, \delta_{n+1}^{n+1}, \phi_{n+1}^{n+1}).$$

The unique solution of this system requires four additional constraints. The boundary data $U_x(a,t)=0$, $V_x(a,t) = 0$ and $U_x(b,t) = 0$, $V_x(b,t) = 0$ can be written in terms of parameters as follows:

$$\delta_{-1} = \delta_1,$$
$$\phi_{-1} = \phi_1,$$
$$\delta_{N-1} = \delta_{N+1},$$
$$\phi_{N-1} = \phi_{N+1}.$$

The parameters $\delta_{-1}, \phi_{-1}, \delta_{N+1}, \phi_{N+1}$ in eq. (10) are from the system by using the relations above obtained from the boundary data to determine a solvable system. In order to initialise the iteration algorithm, the initial parameters δ_j^0, ϕ_j^0, $j = -1, \ldots, N+1$, are determined by using the initial and Neumann boundary conditions:

$$U_x(a,0) = 0 = \delta_{-1}^0 - \delta_1^0,$$
$$U(x_j,0) = \alpha_1\delta_{j-1}^0 + \alpha_2\delta_j^0 + \alpha_1\delta_{j+1}^0 = u(x_j,0), \quad j = 1, \ldots, N-1,$$
$$U_x(b,0) = 0 = \delta_{N-1}^0 - \delta_{N+1}^0,$$
$$V_x(a,0) = 0 = \phi_{-1}^0 - \phi_1^0,$$
$$V(x_j,0) = \alpha_1\phi_{j-1}^0 + \alpha_2\phi_j^0 + \alpha_1\phi_{j+1}^0 = v(x_j,0), \quad j = 1, \ldots, N-1,$$
$$V_x(b,0) = 0 = \phi_{N-1}^0 - \phi_{N+1}^0.$$

3. Stability analysis

The stability of the method is investigated by performing the von Neumann analysis where

$$\delta_m^n = A_1 \xi^n \exp(\mathrm{i}m\omega),$$
$$\phi_m^n = A_2 \xi^n \exp(\mathrm{i}m\omega),$$
$$\rho = \xi^{n+1}/\xi^n. \tag{11}$$

Here, A_1 and A_2 represent the harmonics amplitude. k is the mode number, ρ is the amplification factor and $\omega = kh$. The term $U + U^2$ is assumed as locally constant and replaced κ. Substituting (11) into the system

$$a_1\delta_{m-1}^{n+1} + a_2\delta_m^{n+1} + a_1\delta_{m+1}^{n+1} + \frac{k\kappa}{2}(a_3\delta_{m-1}^{n+1} - a_3\delta_{m+1}^{n+1}) + \frac{k\mu_3}{2}(a_4\phi_{m-1}^{n+1} + a_5\phi_m^{n+1} + a_4\phi_{m+1}^{n+1})$$
$$= a_1\delta_{m-1}^n + a_2\delta_m^n + a_1\delta_{m+1}^n - \frac{k\kappa}{2}(a_3\delta_{m-1}^n - a_3\delta_{m+1}^n) - \frac{k\mu_3}{2}(a_4\phi_{m-1}^n + a_5\phi_m^n + a_4\phi_{m+1}^n), \tag{12}$$

$$a_3\delta_{m-1}^{n+1} - a_3\delta_{m+1}^{n+1} - a_1\phi_{m-1}^{n+1} - a_2\phi_m^{n+1} - a_1\phi_{m+1}^{n+1} = -a_3\delta_{m-1}^n + a_3\delta_{m+1}^n + a_1\phi_{m-1}^n + a_2\phi_m^n + a_1\phi_{m+1}^n \tag{13}$$

gives

$$\xi^{n+1}\left[A_1(2a_1\cos m\omega + a_2) + \frac{A_2 k\mu_3}{2}(2a_4\cos m\omega + a_5) - \mathrm{i}k\kappa A_1 a_3 \sin m\omega\right]$$
$$= \xi^n\left[A_1(2a_1\cos m\omega + a_2) - \frac{A_2 k\mu_3}{2}(2a_4\cos m\omega + a_5) - \mathrm{i}k\kappa A_1 a_3 \sin m\omega\right],$$
$$\frac{\xi^{n+1}}{\xi^n} = \frac{\left[A_1(2a_1\cos m\omega + a_2) - \frac{A_2 k\mu_3}{2}(2a_4\cos m\omega + a_5) - \mathrm{i}k\kappa A_1 a_3 \sin m\omega\right]}{\left[A_1(2a_1\cos m\omega + a_2) + \frac{A_2 k\mu_3}{2}(2a_4\cos m\omega + a_5) - \mathrm{i}k\kappa A_1 a_3 \sin m\omega\right]},$$
$$\rho = \frac{\xi^{n+1}}{\xi^n} = \frac{P_1 + \mathrm{i}Q}{P_2 - \mathrm{i}Q}, \tag{14}$$

where

$$P_1 = A_1\,(2a_1\cos m\omega + a_2) - \frac{A_2 k\mu_3}{2}\,(2a_4\cos m\omega + a_5)\,,$$
$$P_2 = A_1\,(2a_1\cos m\omega + a_2) + \frac{A_2 k\mu_3}{2}\,(2a_4\cos m\omega + a_5)\,,$$
$$Q = k\kappa A_1 a_3 \sin m\omega$$

and

$$\xi^{n+1}\left[-A_2\,(2a_1\cos m\omega + a_2) - 2\mathrm{i}A_1 a_3\sin m\omega\right], = \xi^{n}\left[A_2\,(2a_1\cos m\omega + a_2) + 2\mathrm{i}A_1 a_3\sin m\omega\right], \frac{\xi^{n+1}}{\xi^{n}} = \frac{A_2\,(2a_1\cos m\omega + a_2) + 2\mathrm{i}A_1 a_3\sin m\omega}{-A_2\,(2a_1\cos m\omega + a_2) - 2\mathrm{i}A_1 a_3\sin m\omega} = -1. \tag{15}$$

It can be concluded from both (14) and (15) that $|\rho| \leq 1$. Thus, the proposed method is unconditionally stable.

4. Numerical illustrations

The numerical solutions to some IBVPs set-up with the Gardner equation are summarised in this section. The accuracy of the results determined by the extended B-spline collocation method is discussed by examining graphical representations, measuring the error between the numerical and analytical solutions and the preservation of conservation laws. The error of the numerical solution is measured by using the discrete maximum norm defined as

$$L_\infty(t) = |u(x_j,t) - U(x_j,t)|_\infty = \max_j |u(x_j,t) - U(x_j,t)|,$$

where $U(x_j,t)$ and $u(x_j,t)$ are the numerical and analytical solutions at the discrete time t.

The conservation laws can also be indicators of the validity of the proposed algorithms even when the analytical solution does not exist. The conservation laws of the Gardner equation

$$M = \int_{-\infty}^{\infty} u\,\mathrm{d}x \approx \int_a^b u\,\mathrm{d}x \approx h\sum_{j=0}^{N} u_j,$$
$$E = \int_{-\infty}^{\infty} u^2\,\mathrm{d}x \approx \int_a^b u^2\,\mathrm{d}x \approx h\sum_{j=0}^{N} u_j^2,$$
$$H = \int_{-\infty}^{\infty}\left(\frac{\mu_1 u^3}{3} + \frac{\mu_2 u^4}{6} - \mu_3 (u_x)^2\right)\mathrm{d}x \approx \int_a^b\left(\frac{\mu_1 u^3}{3} + \frac{\mu_2 u^4}{6} - \mu_3 (u_x)^2\right)\mathrm{d}x \approx \sum_{j=0}^{N}\left(\frac{\mu_1 u_j^3}{3} + \frac{\mu_2 u_j^4}{6} - \mu_3 (u_x)_j^2\right) \tag{16}$$

are expected to keep their initial quantities during numerical simulations [26]. The relative changes of these quantities at a discrete time $t > 0$ are measured by using $C(M_t)$, $C(E_t)$ and $C(H_t)$ defined as

$$C(M_t) = \left|\frac{M_t - M_0}{M_0}\right|, \quad C(E_t) = \left|\frac{E_t - E_0}{E_0}\right|, \quad C(H_t) = \left|\frac{H_t - H_0}{H_0}\right|, \tag{17}$$

where M_t, E_t, H_t ($t \geq 0$) are the measured quantities at time t.

4.1 *Propagation of initial single positive pulse*

In the first numerical illustration, we study the propagation of an initial single pulse with positive amplitude. The equation parameters are chosen as $\mu_1 = 4$, $\mu_2 = -3$ and $\mu_3 = 1$. The initial data are determined from the exact solution [19]

$$u(x,t) = \frac{2}{12 + 3\sqrt{14}\cosh\left(-\frac{x}{3} + \frac{5}{3} + \frac{t}{27}\right)}$$

by assuming $t = 0$. As the exact solution approaches zero as x approaches infinity or minus infinity, the choice of the homogeneous boundary conditions is compatible with the solution. The artificial interval $[-20, 30]$ is chosen for the numerical simulation and the designed algorithm is run until time $t = 5$ with the fixed time discretisation parameter $\Delta t = 0.1$ and various spatial discretisation numbers N. The propagation of a positive single solitary wave is given in figure 1.

The error distribution of the extension parameter $\lambda = 0$ and the discretisation parameters $\Delta t = 0.1$ and $N = 100$ at the simulation ending time $t = 5$ is given in figure 2a. The usage of the same discretisation parameters for optimum extension parameter $\lambda = -0.00840$ results in the error distribution at the simulation ending time as shown in figure 2b. A simple comparison shows that the results are improved approximately two times when the optimum extension parameter is used in the algorithm.

The discretised maximum error norms for various values of the grid size are summarised in table 1. In the meanwhile, the algorithm seeks for the optimal value

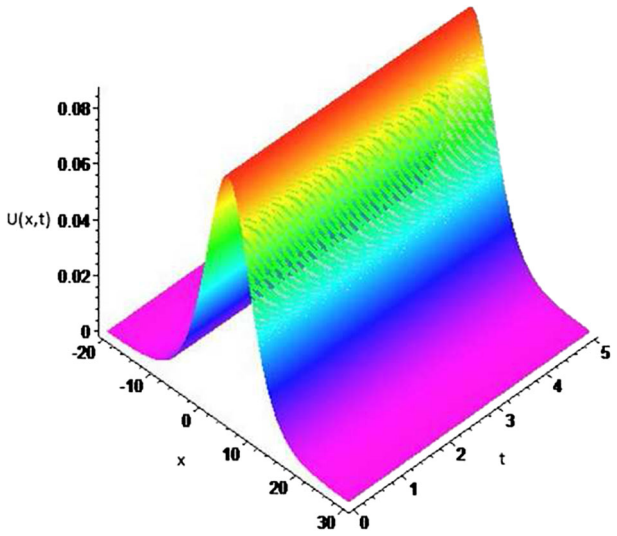

Figure 1. Propagation of a single solitary wave.

of the extension parameter λ by comparing the discrete maximum error norm at each λ. Even though we do not observe an improvement in decimal digits in the results, using the optimum extension parameter λ generates improved results for all choices of N.

The conservation laws are required to preserve their initial values as time proceeds during the simulation. The initial values of these laws are calculated by using Maple (table 2). The absolute relative changes of the conservation laws are obtained for at least six decimal digits at the simulation ending time $t = 5$. These preservation rates can be accepted as indicators of a valid algorithm.

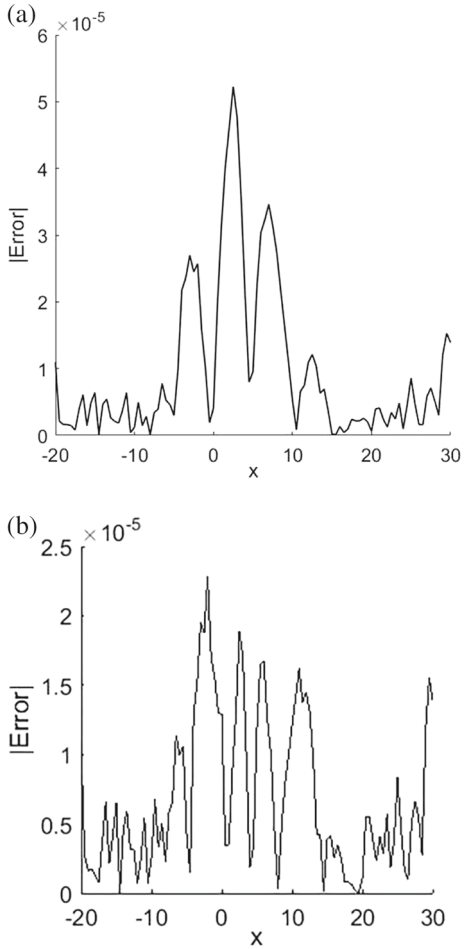

Figure 2. Error distribution of the numerical solution at time $t = 5$: (**a**) error distribution for $\lambda = 0$ at the simulation terminating time and (**b**) error distribution for $\lambda = -0.00840$ at the simulation terminating time.

Table 1. Error norms for various choices of extension parameters.

N	$L_\infty(2.5)(\lambda = 0)$	$L_\infty(2.5)$(various λ)	$L_\infty(5)(\lambda = 0)$	$L_\infty(5)$(various λ)
100	3.272613×10^{-5}	$(\lambda = -0.00840)1.613612 \times 10^{-5}$	5.226060×10^{-5}	2.278972×10^{-5}
200	2.053776×10^{-5}	$(\lambda = -0.00280)1.481971 \times 10^{-5}$	1.916039×10^{-5}	1.911961×10^{-5}
300	1.442848×10^{-5}	$(\lambda = -0.00094)1.250921 \times 10^{-5}$	1.704034×10^{-5}	1.713378×10^{-5}
400	1.445279×10^{-5}	$(\lambda = -0.00178)1.443999 \times 10^{-5}$	1.611496×10^{-5}	1.587201×10^{-5}

Table 2. Calculated conservation laws and their absolute relative changes.

N	M_0	E_0	H_0	$C(M_5)$	$C(E_5)$	$C(H_5)$
100	1.044585	0.060134	0.004070	5.474878×10^{-6}	3.817601×10^{-8}	1.523304×10^{-6}
200	1.044586	0.060134	0.004070	3.266987×10^{-6}	5.112634×10^{-8}	1.700390×10^{-6}
300	1.044586	0.060134	0.004070	2.419017×10^{-7}	2.176765×10^{-8}	2.835162×10^{-6}
400	1.044587	0.060134	0.004070	1.375331×10^{-6}	2.091049×10^{-10}	3.393931×10^{-6}

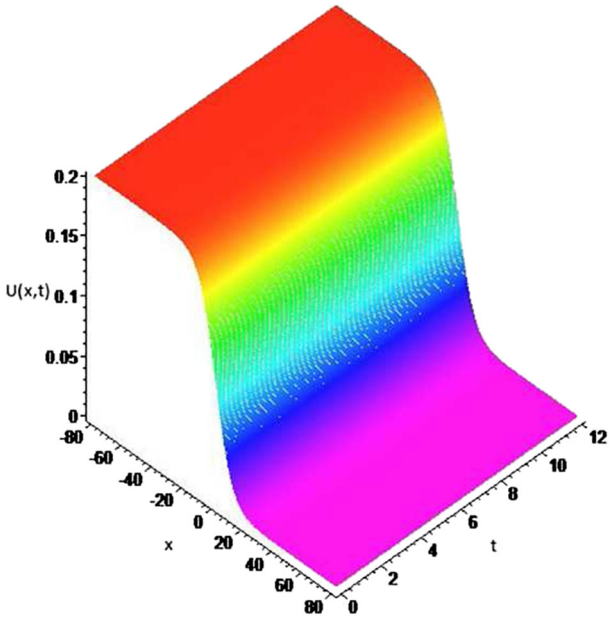

Figure 3. Propagation of a single solitary wave.

4.2 *Propagation of kink-like wave*

The kink-like wave solution of the Gardner equation is

$$u(x,t) = \frac{1}{10} - \frac{1}{10}\tanh\left(\frac{\sqrt{30}}{60}\left(x - \frac{1}{30}t\right)\right) \qquad (18)$$

for the equation parameters $\mu_1 = 1$, $\mu_2 = -5$ and $\mu_3 = 1$ [27]. This wave propagates along the x-axis with the speed $1/30$. The initial data are generated from the analytical solution by assuming $t = 0$. Since the analytical solution disappears as $x \to \infty$ and $u(x,t) \to 0.2$ as $x \to -\infty$, the homogeneous Neumann data are compatible. The artificial problem interval is chosen as $[-80, 80]$ and the designed algorithm is run up to the ending time $t = 12$ with $\Delta t = 0.1$ and various grid numbers used in the space domain. The plot in figure 3 is a summary of the propagation in this finite interval.

The designed algorithm is scanned for the extension parameter in $[-1, 1]$ with step size $\Delta\lambda = 0.000001$ for an optimum value to improve the results. The optimum extension parameters are determined for all choices of the number of grids (table 3 and figure 4). The determination of the optimum extension parameter reduces the maximum absolute error to half for all choices of N.

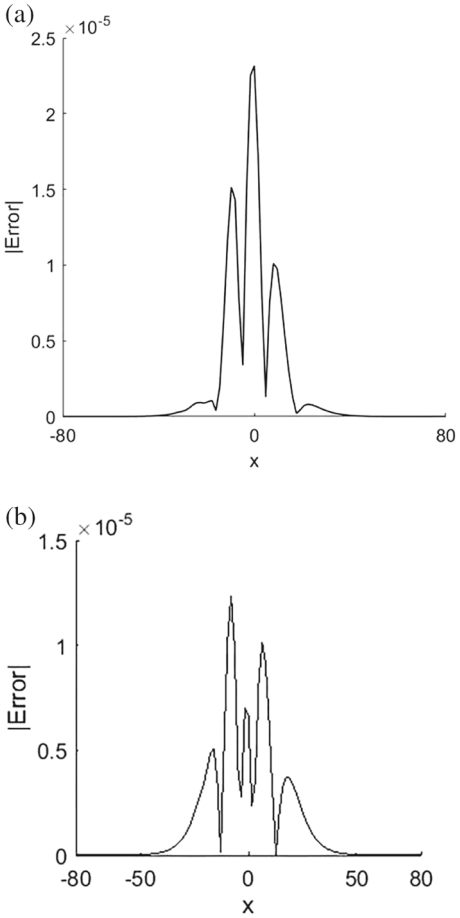

Figure 4. Error distribution of the numerical solution at time $t = 12$: (**a**) error distribution for $\lambda = 0$ at the simulation terminating time and (**b**) error distribution for $\lambda = -0.01850$ at the simulation terminating time.

The initial values of the conservation laws are calculated on the integration of the quantities by substituting the initial data of the IBVP. The absolute relative changes of the conservation laws indicate a reliable solution in table 4.

Table 3. Error norms for optimum choices of extension parameters.

N	$L_\infty(4)(\lambda = 0)$	$L_\infty(4)$(various λ)	$L_\infty(12)(\lambda = 0)$	$L_\infty(12)$(various λ)
100	8.415049×10^{-6}	$(\lambda = -0.01850)3.397351 \times 10^{-6}$	2.315818×10^{-5}	$(\lambda = -0.01850)1.233048 \times 10^{-5}$
200	2.120684×10^{-6}	$(\lambda = -0.00574)1.019380 \times 10^{-6}$	5.995606×10^{-6}	$(\lambda = -0.00574)2.966350 \times 10^{-6}$
400	5.329656×10^{-7}	$(\lambda = -0.00115)2.544051 \times 10^{-7}$	1.501551×10^{-6}	$(\lambda = -0.00115)7.739716 \times 10^{-7}$
600	2.367741×10^{-7}	$(\lambda = -0.000584)1.134974 \times 10^{-7}$	6.665529×10^{-7}	$(\lambda = -0.000584)3.408862 \times 10^{-7}$

Table 4. Calculated conservation laws and their absolute relative changes.

N	M_0	E_0	H_0	$C(M_{12})$	$C(E_{12})$	$C(H_{12})$
100	16.159999	3.012911	0.097996	4.950519×10^{-3}	5.310572×10^{-3}	5.442433×10^{-3}
200	16.079999	2.996911	0.097462	4.975152×10^{-3}	5.339086×10^{-3}	5.472739×10^{-3}
400	16.039999	2.988911	0.097195	4.987546×10^{-3}	5.353658×10^{-3}	5.487727×10^{-3}
600	16.026666	2.986244	0.097107	4.991690×10^{-3}	5.358780×10^{-3}	5.493035×10^{-3}

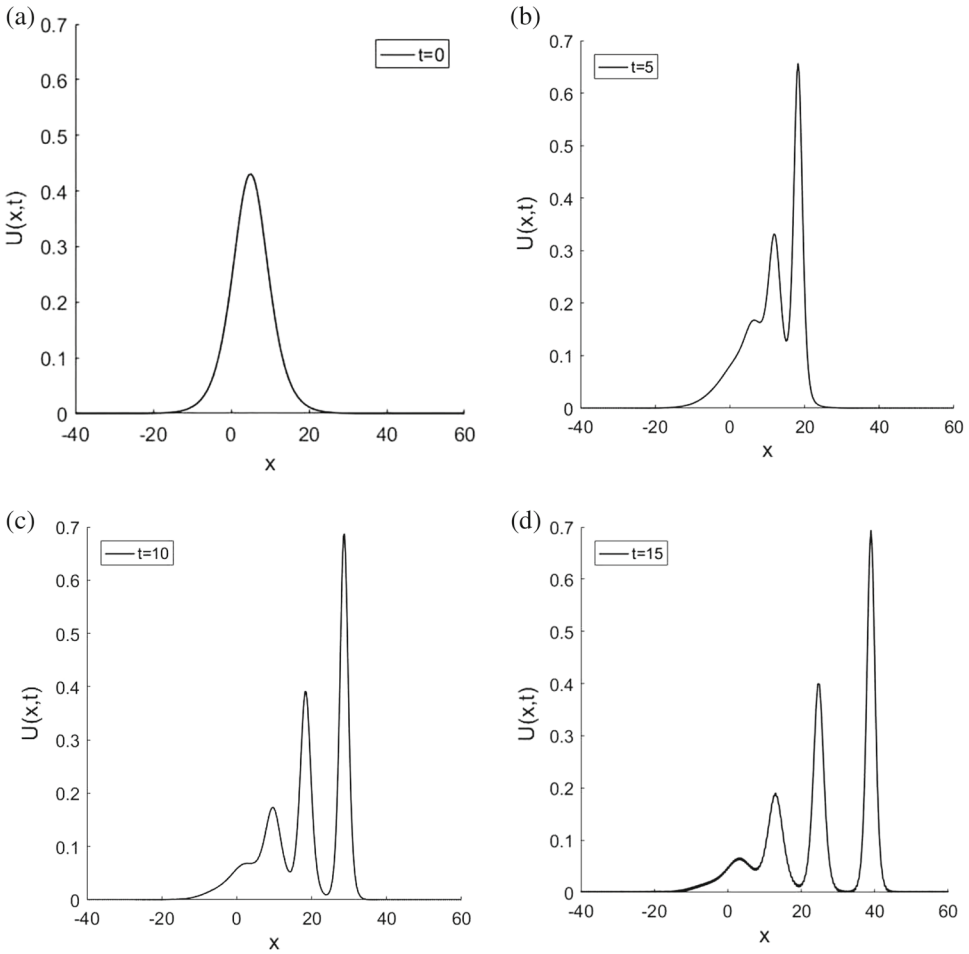

Figure 5. Wave generation from an initial positive pulse: (**a**) initial data, (**b**) $t = 5$, (**c**) $t = 10$ and (**d**) $t = 15$.

4.3 *Wave generation from an initial pulse*

The perturbed Gardner equation of the form

$$u_t + \mu_1 u u_x + \mu_2 u^2 u_x + \mu_3 u_{xxx} + \epsilon = 0 \tag{19}$$

for some non-zero real ϵ can be useful to study the wave generation from an initial positive pulse. The initial data are chosen as

$$u(x,t) = \frac{2}{3}\frac{1}{4 + \sqrt{14}\cosh\left(\frac{x}{3} - \frac{5}{3}\right)} \tag{20}$$

with the parameters $\mu_1 = 10$, $\mu_2 = -3$ and $\mu_3 = 1$ in the Gardner equation (19). The designed program is run in the finite interval $[-40, 60]$ with the parameters $N = 400$ and $\Delta t = 0.01$ up to $t = 15$. The initial positive pulse of height 0.4305 positioned at $x = 5$ propagates along the x-axis (figure 5a). When the propagation time reaches $t = 5$, a frontier wave of height 0.6568 is positioned at $x = 18.25$ (figure 5b). The first follower solitary wave is clearly observable at this time. This follower is of height 0.3318 and it is positioned at $x = 12$. Even though it is not clearly observable, a bulge at the left of the first follower can be evaluated as an indicator of a second follower wave. The first three

Table 5. Calculated conservation laws and their absolute relative changes.

t	M_0	E_0	H_0	$C(M_t)$	$C(E_t)$	$C(H_t)$
5	5.225502	1.503363	1.599480	8.071923×10^{-7}	3.058803×10^{-5}	1.288666×10^{-3}
10	5.225502	1.503363	1.599480	2.765201×10^{-6}	4.134255×10^{-5}	1.848560×10^{-3}
15	5.225502	1.503363	1.599480	7.038028×10^{-6}	6.113201×10^{-4}	2.157111×10^{-3}

waves are clearly observable at $t = 10$ (figure 5c). The height of the frontier reaches 0.6871 and its peak point is positioned at $x = 28.75$. The peak of the first follower wave of height 0.3913 is positioned at $x = 18.25$. At the left of the first follower, almost completely formed second follower of height 0.1736 is positioned at $x = 9.75$. The height of the frontier is measured as 0.6941 at time $t = 15$ (figure 5d). Its peak is positioned at $x = 39$ at this time. The height of the first follower wave reaches 0.3998 and its peak position is measured as $x = 24.75$. The second follower of height 0.1910 is positioned at $x = 13$. The bulge appearing at the left of the second follower is the indicator of the formation of one more solitary.

Even though we cannot compare the results with the analytical solutions, the absolute relative changes of the conservation laws are a good indicator to evaluate the efficiency of the proposed method. The initial values of the conservation laws and their absolute relative changes are summarised in table 5 for $\lambda = 0$. The absolute relative change of the first conservation law is only in six decimal digits, the second one in four decimal digits and the third one in three decimal digits at the simulation ending time $t = 15$.

5. Conclusion

The extended cubic B-spline collocation method is constructed for some initial boundary value problems for the Gardner equation. The scan of the optimum extension parameter in the interval $[-1, 1]$ may give opportunity to obtain more reliable results when comparing classical cubic B-splines when $\lambda = 0$. As the extended cubic B-splines have only first- and second-order derivatives, the reduction in the order of the third-order derivative is required. Thus, the coupled system of nonlinear PDEs is obtained. The extended B-spline function is used to approximate the solutions of this system. Following the spatial discretisation, the linearisation procedure is followed. After the time discretisation carried out using the Crank–Nicolson method, linearisation is applied to have linear coupled system. This system is fully discretised by way of the extended collocation procedure. System is shown to be stable with the application of the von Neumann stability analysis.

The first two examples give opportunity to measure the error between the analytical and numerical solutions by calculating maximum error norms for various choices of the discretisation parameters. Both the graphical representations and absolute relative changes of the conservation laws are indicators of a reliable and valid method. In our study, the results have not improved much when the optimum numerical values are searched by scanning which is predetermined in the interval $[-1, 1]$.

In the third example, a non-analytical problem simulating wave generation from an initial single solitary wave is studied. The proposed algorithm simulates the expected results successfully. The absolute relative changes of the conservation laws confirm the valid results.

Acknowledgements

This study is a part of the project with number 2016/19052 supported by the Eskisehir Osmangazi University Scientific Research Projects Committee and was partially presented at the Third International Conference on Pure and Applied Sciences, Dubai, 2017.

References

[1] E Demler and A Maltsev, *Ann. Phys*. **326**, 1775 (2011)
[2] M S Ruderman, T Talipova and E Pelinovsky, *J. Plasma Phys*. **74**, 639 (2008)
[3] A M Kamchatnov, Y H Kuo, T C Lin, T L Horng, S C Gou, R Clift, G A El and R H Grimshaw, *Phys. Rev. E* **86**, 036605 (2012)
[4] R Grimshaw, E Pelinovsky, T Taipova and A Sergeeva, *Eur. Phys. J. Special Top*. **185**, 195 (2010)
[5] A M Kamchatnov, Y H Kuo, T C Lin, T L Horng, S C Gou, R Clift, G A El and R H Grimshaw, *J. Fluid Mech*. **736**, 495 (2013)
[6] A V Slyunyaev and E N Pelinovski, *J. Exp. Theor. Phys*. **89**, 173 (1999)
[7] H Hu, M Tan and X Hu, *J. Assoc. Arab Univ. Basic Appl. Sci*. **21**, 64 (2016)
[8] Y Wei-Feng, L Sen-Yue, Y Jun and H Han-Wei, *Chin. Phys. Lett*. **31**, 070203 (2014)
[9] A Biswas and E Zerrad, *Adv. Stud. Theor. Phys*. **2**, 787 (2008)

[10] Y Jia-Ren, P Liu-Xian and Z Guang-Hui, *Chin. Phys. Lett*. **17**, 625 (2000)
[11] J B Zhou, J Xu, J D Wei and X Q Yang, *Pramana – J. Phys*. **88**: 69 (2017)
[12] A Bekir, *Commun. Nonlinear Sci. Numer. Simul*. **14**, 1038 (2009)
[13] Z Fu, S Liu and S Liu, *Chaos Solitons Fractals* **20**, 301 (2004)
[14] H L Lü, X Q Liu and L Niu, *Appl. Math. Comput*. **215**, 3811 (2010)
[15] M A Akbar, N Hj and M Ali, *World Appl. Sci. J*. **17**, 1603 (2012)
[16] H Naher and F A Abdullah, *World Appl. Sci. J*. **16**, 1559 (2012)
[17] A J A M Jawad, *Studies Math. Sci*. **5**, 13 (2012)
[18] N Taghizade and A Neirameh, *Int. J. Nonlinear Sci*. **9**, 305 (2010)
[19] A M Wazwaz, *Commun. Nonlinear Sci. Numer. Simul*. **12**, 1395 (2007)
[20] H Nishiyama and T Noi, *Comput. Appl. Math*. **35**, 75 (2016)
[21] T M Rageh, G Salem and F A El-Salam, *Int. J. Adv. Appl. Math. Mech*. **1**, 1 (2014)
[22] N M Yagmurlu, O Tasbozan, Y Ucar and A Esen, *Appl. Math. Inf. Sci. Lett*. **4**, 19 (2016)
[23] A Aydin and C Koruoglu, *Pramana – J. Phys*. **89**: 72 (2017)
[24] O Oruç, F Bulut and A Esen, *Pramana – J. Phys*. **87(6)**: 94 (2016)
[25] S G Rubin and R A Graves, *Cubic spline approximation for problems in fluid mechanics* (Nasa TR R-436, Washington, DC, 1975)
[26] S Hamdi, B Morse, B Halphen and W Schiesser, *Nat. Hazards* **57**, 609 (2011)
[27] A Wazwaz, *Partial differential equations and solitary waves theory* (Springer-Verlag, Berlin, Heidelberg, 2009)